

Article

Simulated Ageing of Crude Oil and Advanced Oxidation Processes for Water Remediation since Crude Oil Pollution

Filomena Lelario ¹, Giuliana Bianco ¹ , Sabino Aurelio Bufo ^{1,2,*}  and Laura Scrano ³ 

¹ Department of Sciences, University of Basilicata, Via dell'Ateneo Lucano 10, 85100 Potenza, Italy; filomena.lelario@unibas.it (F.L.); giuliana.bianco@unibas.it (G.B.)

² Department of Geography, Environmental Management & Energy Studies, University of Johannesburg, Johannesburg 2092, South Africa

³ Department of European Cultures (DICEM), University of Basilicata, 75100 Matera, Italy; laura.scrano@unibas.it

* Correspondence: sabino.bufo@unibas.it; Tel.: +39-0971-6237

Abstract: Crude oil can undergo biotic and abiotic transformation processes in the environment. This article deals with the fate of an Italian crude oil under simulated solar irradiation to understand (i) the modification induced on its composition by artificial ageing and (ii) the transformations arising from different advanced oxidation processes (AOPs) applied as oil-polluted water remediation methods. The AOPs adopted were photocatalysis, sonolysis and, simultaneously, photocatalysis and sonolysis (sonophotocatalysis). Crude oil and its water-soluble fractions underwent analysis using GC-MS, liquid-state ¹H-NMR, Fourier transform ion cyclotron resonance mass spectrometry (FT-ICR-MS), and fluorescence. The crude oil after light irradiation showed (i) significant modifications induced by the artificial ageing on its composition and (ii) the formation of potentially toxic substances. The treatment produced oil oxidation with a particular effect of double bonds oxygenation. Non-polar compounds present in the water-soluble oil fraction showed a strong presence of branched alkanes and a good amount of linear and aromatic alkanes. All remediation methods utilised generated an increase of C₅ class and a decrease of C₆-C₉ types of compounds. The analysis of polar molecules elucidated that oxygenated compounds underwent a slight reduction after photocatalysis and a sharp decline after sonophotocatalytic degradation. Significant modifications did not occur by sonolysis.

Keywords: crude oil; photocatalysis; sonolysis; sonophotocatalysis; FT-ICR/MS; Kendrick plot; van Krevelen diagram; water; pollution; remediation



Citation: Lelario, F.; Bianco, G.; Bufo, S.A.; Scrano, L. Simulated Ageing of Crude Oil and Advanced Oxidation Processes for Water Remediation since Crude Oil Pollution. *Catalysts* **2021**, *11*, 954. <https://doi.org/10.3390/catal11080954>

Academic Editor: Fernando J. Beltrán Novillo

Received: 13 July 2021

Accepted: 4 August 2021

Published: 10 August 2021

Publisher's Note: MDPI stays neutral with regard to jurisdictional claims in published maps and institutional affiliations.



Copyright: © 2021 by the authors. Licensee MDPI, Basel, Switzerland. This article is an open access article distributed under the terms and conditions of the Creative Commons Attribution (CC BY) license (<https://creativecommons.org/licenses/by/4.0/>).

1. Introduction

The composition of petroleum crude oil varies widely depending on the source and processing. Oil is a complex organic mixture counting for a high number of chemically distinct components, including unsaturated and saturated hydrocarbons, hetero-atoms (such as N, S, and O) and a minor percentage of metals predominantly vanadium, nickel, iron, and copper. Many oil constituents can be carcinogens, neurotoxins, respiratory irritants, hepatotoxins, nephrotoxins, and mutagens. Their toxic effects can be acute and chronic, causing many direct symptoms and major long-term injuries, including reproductive problems and cancer [1].

The hydrocarbon fraction can be as high as 90% by weight in light oils, compared to about 70% in heavy crude oil. A majority of the heteroatomic free constituents are side-by-side paraffinic chains, naphthalene rings, and aromatic rings. Heteroatomic compounds constitute a relatively small portion of crude oils, less than 15%. However, they have significant implications since their presence, composition, and solubility, which depend on the origin of the crude oil, can cause either positive or negative effects in the transformation processes and are of environmental concern [2,3].

A significant consideration of the several processes affecting the crude oil spilled into the environment is needed to clarify the effects of increasingly widespread harmful events and

predict the future fate of the oil. For this reason, the awareness of such phenomena will prove to be a valuable resource in the effort to develop innovative remediation technologies. The ecological impact of oil contamination in different environmental sections (marine, terrestrial and atmospheric) is a source of severe concern. Extraction techniques, transportation and refinery treatments of crude oil can originate pollution phenomena due to the dispersion of these compounds everywhere. These problems have attracted significant attention to understanding the fate of oil in the environment and the natural mechanisms of oil degradation and transformation to suggest a method to reduce the damages caused by original and derivative products [4–6].

As all xenobiotic substances, crude oil undergoes biotic (biotransformation by aquatic organisms such as algae, bacteria) and abiotic (hydrolysis, oxidation, photodegradation) processes, giving rise to many derivatives. In the same way as their parent molecules, these transformation products can lead to the contamination of terrestrial and aquatic environments due to oil deposition on soil and into the surface- and ground-water. Nevertheless, they can be more persistent and toxic than the parent compounds [1–3].

Extensive literature is already available on the microbiological degradation of crude oil, which received considerable attention from researchers. For example, since 1975, the biodegradability of crude oils has been studied and found to be highly dependent on their composition and incubation temperature [5]. Researchers also examined the ability of microorganisms to degrade a high number of hydrocarbons of a different structure in petroleum [6]. Furthermore, many authors have elucidated that the lighter fractions can undergo degradation more rapidly than the heavier ones, e.g., n-alkanes degraded more quickly than branched alkanes, and aromatics with two to three rings readily biodegraded through several pathways [4–8].

Photochemical processes are also essential contributors to pollutants' degradation and the removal of exogenous substances from the environment [9,10], especially in tropical and sub-tropical climates. In those areas, solar irradiation intensity is high, and the lack of nutrients hinders biological processes. Moreover, photochemical reactions are the primary cause of the compositional change of crude oil spilt in a marine environment [11–13]. Photolysis plays an essential role in the mousse formation that begins a few moments after an oil spill [12]. Due to sunlight, the interfacial tension of a crude oil film rapidly decreases, and chocolate mousse starts to form, which leads to the stabilisation of the water-in-oil emulsions [13,14]. The formation of emulsions seems to depend on the amount of asphaltene present in the oil film, and researchers reported that this amount increases upon irradiation [13]. Moreover, an increase in emulsion viscosity occurs due to the structural organisation of the asphaltenes [14].

The oxidised products resulting from the photochemical transformation significantly affect the viscosity, mousse formation, and weathered petroleum's physical properties. Moreover, photo-oxidation can lead to the destruction of existing toxic components, the generation of new toxic constituents and the formation of water-soluble products [10–14].

Since crude oil settles on the surface of water and soil, it undergoes solar irradiation. Solar degradation is a natural way for petroleum decontamination, also suggesting that techniques based on light irradiation could be helpful to the petroleum degradation processes. Light irradiation-based technologies have been improved using catalysts, the most effective and cheapest water purification tool being titanium dioxide (TiO_2) [15,16]. Researchers have exploited combinations of different advanced oxidation processes (AOPs) for environmental detoxification in the last years, especially for wastewater treatment. The so-called sonophotocatalysis (SPC), the simultaneous use of ultrasound (US) and photocatalysis (PC) by semiconductors to degrade organic pollutants in water (e.g., the effluent of dye works) has been investigated, but combined AOPs methods were not applied to oil-polluted water remediation to our knowledge [17–22].

Among the analytical techniques available for structurally determining crude oil components or metabolites, gas chromatography combined with mass spectrometry (GC-MS) has been the best choice so far and most widely used [23,24]. The fractionation of crude

oil and subsequent GC-MS analysis has characterised nearly 300 components comprising aliphatic, aromatic, and biomarker compounds [25–28]. However, most crude oil fractions remain unidentified since many components cannot be resolved and appear as “hump” or “unresolved complex mixture (UCM)” in GC chromatograms [29,30].

Compositions of the saturated hydrocarbons have been better characterised by two-dimensional gas chromatography coupled to mass spectrometry [29] and liquid chromatography-mass spectrometry [31]. However, polar species appear poorly resolved due to their compositional complexity far exceeding the peak capacity of typical analytical techniques. High mass resolving power is necessary for the resolution of many compounds present in crude oil.

The development of Fourier transform ion cyclotron resonance mass spectrometry (FT-ICR MS) had provided the needed ultra-high resolving power ($m/\Delta m_{50\%} > 100,000$, in which $\Delta m_{50\%}$ is peak width at half peak height), and the use of electrospray ionization (ESI) mass spectrometry had made possible to detect most polar species. Thus, the coupling of these two techniques, ESI and FT-ICR mass spectrometry, produces a powerful analytical tool for analysing these polar species without a preliminary chromatographic separation [32,33].

This work investigates the modifications that the artificial ageing induced on the composition of the polar fraction of an Italian crude oil (Basilicata region—Southern Italy, Val D’Agri countryside) under solar irradiation. Moreover, it explores the possibility of oil-polluted water remediation using AOPs, such as photocatalysis (UV + TiO₂), sonolysis (US, ultrasound irradiation) and the simultaneous use of photocatalysis and sonolysis, i.e., sonophotocatalysis (UV + TiO₂ + US).

2. Results and Discussion

The crude oil sample, collected from the Oil Centre sited in Val D’Agri (Basilicata), underwent simulated solar treatment. Information on the composition of the oil water-soluble fraction obtained through GC-MS, liquid state ¹H NMR and FT-ICR-MS was the basis for this investigation. Liquid state ¹H NMR spectroscopy accomplished helpful information on the oil composition. This technique recognised amounts of 59%, 19%, and 20% of total hydrocarbons as linear, cyclic (or branched), and aromatic compounds. NMR spectroscopy cannot discriminate branched from cyclic alkanes because both compounds have the same intramolecular environment. Figure S1 compares data obtained by NMR and GC-MS.

The use of real standards introduced by an electrospray ion source allowed the calibration of mass spectra. Recalibration was necessary for the identified homologous series in each sample [34]. A troubling complication in structural studies of crude oil has been its enormous complexity on a molecular scale. The ultrahigh-resolution of FT-ICR spectra can be highly complex: these spectra typically comprise many peaks at each “Nominal mass” and thousands of peaks in a whole spectrum. Each peak could represent a chemically diverse compound. This complexity poses an investigative challenge to the study of spectra for structural interpretation.

The univocal assignment of elementary composition, merely based on the high resolution and accuracy of the instrument, is not possible for all mass values. For values higher than 400–500 Da, it is necessary to validate the result differently. The Kendrick plot (Kendrick mass defect vs Kendrick Nominal mass or KMD vs KNM) offers an outstanding vehicle to visualise and categorise all of the peaks in a mass spectrum. Kendrick mass defect (KMD) breakdown has been effectively applied to ultra-high resolution mass spectra, consenting to categorise peaks into complex spectra based on their homologous similarities across a selected type of masses [35]. Bi-dimensional plots can discern compounds differing by masses associated with a structural unit (e.g., CH₂, COOH, CH₂O, etc.). In this drawing, the signals of structurally related moieties all lie on horizontal or diagonal straight lines. Such a method permits the extraction of peaks that are homogeneously associated. The method can effectively recognise groups of associated compounds in FT-ICR-MS of

petroleum samples [36]. The compounds of the same homologous series (having a different number of groups CH₂) will fall in a single horizontal line of the diagram (KNM), with peaks separated from 14 Da and no difference of KMD.

Similarly, the signals relating to compounds of the same class but of different types will occupy points on a vertical line of the diagram, separated by a difference of 0.013 in the Kendrick mass defect. The conversion of mass spectra from the IUPAC mass scale (based on the ¹²C atomic mass as exactly 12 Da) to the Kendrick mass scale is the first step. The Kendrick mass scale poses CH₂ = 14.0000 Da rather than 14.01565 Da. The Kendrick mass comes from the IUPAC mass, as shown in Equation (1) [35,36]:

$$\text{Kendrick mass} = \text{IUPAC mass} \times (14.00000/14.01565) \quad (1)$$

Members of a homologous series (specifically, compounds that comprehend the same heteroatom and number of rings plus double bonds, but a different number of CH₂ groups) have the same KMDs. They are thus quickly organised and selected from a list of all detected ion masses, as shown in Equation (2):

$$\text{KMD} = \text{KNM} - \text{KEM} \quad (2)$$

where KEM is the Kendrick exact mass.

By rounding the Kendrick mass up to the nearest whole number, the nominal Kendrick mass conveniently arises. Next, homologous series are parted based on even and odd Kendrick Nominal mass and KMD, as described elsewhere [36,37]. Finally, the Kendrick masses are sorted based on Kendrick mass defect and nominal-Z value and exported into an Excel spreadsheet in the second step. Then, a molecular formula calculator programme, limited to molecular formulas consisting of up to ¹²C 0–80 and ¹⁶O 0–10, assigns elemental compositions. Since members of a homologous series diverge only by integer multiples of CH₂, the assignment of a single unit of such a series typically suffices to identify all higher-mass members of that series [36].

We also used the van Krevelen diagram for examining ultra-high resolution mass spectra. This kind of layout is used broadly in the geochemistry literature to study the evolution of coals or oil samples [38–40]. The molar hydrogen-to-carbon ratios (H/C) constitute the ordinate, and the molar oxygen-to-carbon ratio (O/C), the abscissa. As a result, each class of compounds plots in a specific location on the diagram. Researchers well recognised that they can identify the type of compounds from the position of their representative points in the van Krevelen plot [41–43].

In general, the chemical formula CcH2c(Z)NnOoSs can identify the crude oil composition. That is because the hydrogen deficiency index <Z> of the molecule is the same for all members of a homologous “type” series (i.e., the fixed number of rings plus double bonds). Every two-units decrease in <Z> value represents the addition of one ring or a double bond. Therefore, number-average molecular weight, *M_n*, and weight-average molecular weight *M_w* have a synthetic definition as:

$$M_n = \sum i M_i / \sum N_i \quad (3)$$

and

$$M_w = \sum N_i M_i^2 / \sum N_i M_i \quad (4)$$

where *N_i* is the relative abundance of ions of mass *M_i* [34].

The <Z> number plays an essential role for the general molecular formula CcH2c(Z)X of the corresponding neutral species, in which X denotes the constituent heteroatom (Nn, Oo, and Ss).

2.1. Ageing Study of Crude Oil by FT-ICR-MS

A solar simulator (Suntest®), equipped with a xenon lamp as the light source used for the ageing treatment, provided information about the crude oil's photochemical behaviour.

GC-MS spectra showed that the fraction present in the highest percentage shifted from the C₈–C₁₁ fractions to the C₁₃ (Figure S2) in the irradiated sample. We observe an increased amount of the C₁₃–C₂₃ and a decreased amount of the C₇–C₁₂ fractions. In the natural (not irradiated) oil, the C₈–C₁₁ fractions represented 54.8% of all the compounds detected. Figure S2B depicts the distribution of the compounds as a function of their chemical type. The GC-MS analysis of the mixture deriving from solar simulator irradiation showed an increase in the relative amounts of both linear alkanes and aromatic compounds. At the same time, we observed a sharp decrease in the relative amounts of branched chains. After irradiation, we did not find cyclic alkanes and alkenes.

After the irradiation, the compositional analysis of the linear alkanes highlighted several changes (Figure S2C) compared to the not irradiated sample. Undecane was the hydrocarbon found in the highest percentage in the crude oil, while pentadecane was in the irradiated oil. A decrease in the C₇–C₁₂ and an increase in C₁₃–C₂₅ fractions is evident. All our analytical determinations agree with reducing the number of branched alkanes in crude oil after irradiation. Figure S2D illustrates the modifications of the composition of this fraction. After the irradiation, branched alkanes underwent a sharp reduction and only C₈, C₉, C₁₁, C₁₂, and C₁₃ fractions were present. Cyclic alkanes were not present after the solar simulator experiment (Figure S2E).

The percentage area of the aromatic compounds did not vary with solar irradiation (Figure S2B). However, a sharp decrease in benzene-like structures and an increase in naphthalenic ones have been observed (Figure S2F).

Figure 1a,b show the FT ICR-MS spectra of untreated and treated crude oil, respectively. The spectra show the distribution of multiple ions with a single charge comprised between m/z 150 and m/z 1400. Figure 1(c₁–c₃) show the scale-expanded segment of the mass spectrum in Figure 1a, revealing an average period of nominal 14 mass units. The signal intensities increased after light irradiation. The shift of maximum apex was not negligible in the treated crude oil sample, which was also more viscous. Thanks to the high accuracy of mass and the excellent resolution power of FT-ICR-MS, it was possible to carry out the non-ambiguous determination of the elementary composition of multiple isobaric picks.

The chemical formula C_cH_{2c(Z)}X generally expresses the composition of a hydrocarbon molecule; where, <c> is the number of carbon atoms, <Z> is the hydrogen deficiency (a measure of aromatic character), and X represents the constituent heteroatom (N, S, O) in the molecule. The heteroatom of interest is oxygen in this study. For simplification, Kendrick and van Krevelen diagrams of natural and irradiated crude oil shown in the figures report only the O₃ class, which contains the most numerous groups of detected ions. Table 1 illustrates an example of homologous series extracted by the mass spectrum of the untreated sample, with a degree of unsaturation $Z = -20$ and class of oxygen O₃, containing the most numerous groups of detected ions.

The compounds of the same homologous series, having a different number of CH₂ groups, fall in a single horizontal line of the Kendrick plot with peaks separated from 14 Da and no difference in the Kendrick mass defect (Table 1, Figure 2). The compounds of the same class but different typology settle down on a vertical line of the diagram separated from a difference of 0.0134 in the value of KMD. Figure 2 compares Kendrick plots for positive-ion ESI FT-ICR mass spectra of natural (■) and irradiated (X) crude oil samples. Due to the high number of signals, the figure reports only the O₃ class, containing the most numerous group of detected ions. Kendrick plot of crude oil sample for O₃ class shows many compounds with a high degree of unsaturation (high value of KMD). In the low values of KMD, the highest percentage of compounds has a small alkylation series (limited number of -CH₂- moieties).

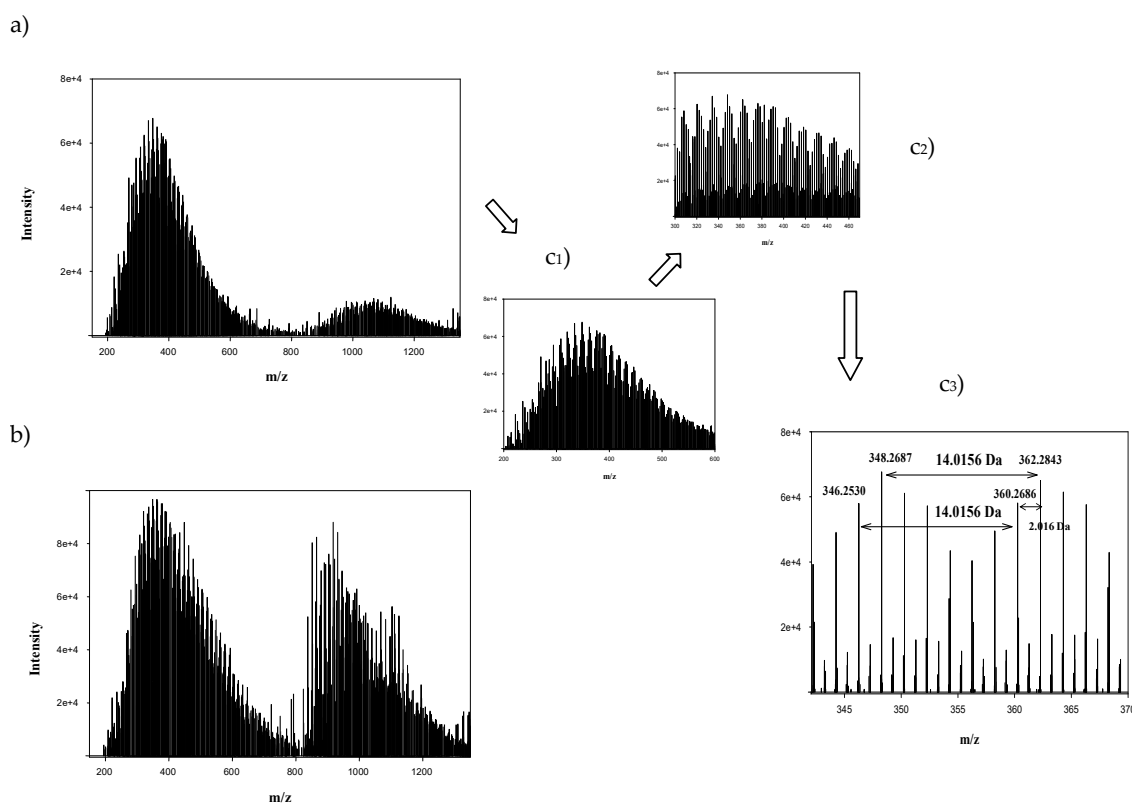


Figure 1. (a) FT ICR-MS spectrum of the untreated oil sample; (b) FT ICR-MS spectrum of the same sample irradiated by xenon-lamp. The spectrum shows the distribution of multiple ions with a single charge comprised between m/z 150 and 1400; c_1 , c_2 , c_3 insets = mass scale-expanded segments of the full range crude oil mass spectrum in Figure 1a, revealing periodicities of 14.016 Da from compound series differing in the number of CH_2 groups and 2.016 Da from compound series differing in the number of rings plus double bonds.

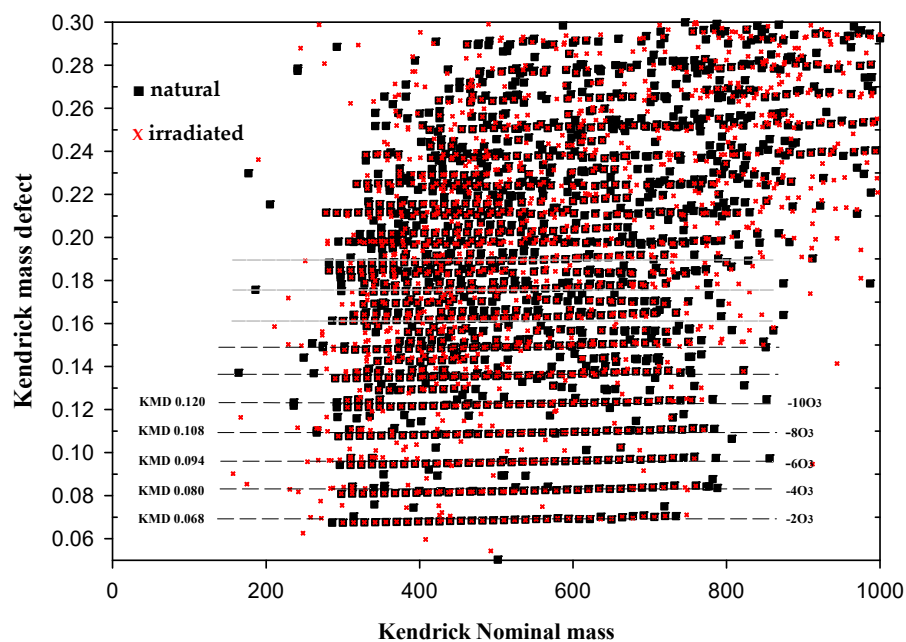


Figure 2. Kendrick mass plot of the O_3 species found in natural (■) and irradiated oil (X). This plot illustrates the increase in the number of rings plus double bonds as the KMD increases (y -axis) and the alkylation series along the x -axis.

Table 1. Homologous series of O₃ class with <Z> = −20.

m/z	Intensity	Composition	KNM	KMD
337.1818	3941.7	C ₂₂ H ₂₅ O ₃	4721	0.45494
351.1972	5150.2	C ₂₃ H ₂₇ O ₃	4917	0.23920
365.2128	3112.4	C ₂₄ H ₂₉ O ₃	5113	0.02038
379.2270	4609.2	C ₂₅ H ₃₁ O ₃	5310	0.82256
393.2424	4252.4	C ₂₆ H ₃₃ O ₃	5506	0.60640
407.2582	3311.8	C ₂₇ H ₃₅ O ₃	5702	0.38464
421.2737	3427.8	C ₂₈ H ₃₇ O ₃	5898	0.16848
435.2893	4966.3	C ₂₉ H ₃₉ O ₃	6095	0.94924
449.3052	3587.2	C ₃₀ H ₄₁ O ₃	6291	0.72748
463.3202	4252.1	C ₃₁ H ₄₃ O ₃	6487	0.51692
477.3362	4772.3	C ₃₂ H ₄₅ O ₃	6683	0.29390
505.3668	7455.6	C ₃₄ H ₄₉ O ₃	7076	0.86536
533.3981	5506.9	C ₃₆ H ₅₃ O ₃	7468	0.42618
547.4131	6265.8	C ₃₇ H ₅₅ O ₃	7664	0.21674
561.4292	6183.2	C ₃₈ H ₅₇ O ₃	7861	0.99120
575.4446	5847.4	C ₃₉ H ₅₉ O ₃	8057	0.77504
589.4606	5685.7	C ₄₀ H ₆₁ O ₃	8253	0.55118
603.4760	6234.8	C ₄₁ H ₆₃ O ₃	8449	0.33586
617.4921	5529.1	C ₄₂ H ₆₅ O ₃	8645	0.11018
631.5075	3522.3	C ₄₃ H ₆₇ O ₃	8842	0.89486
645.5230	4399.5	C ₄₄ H ₆₉ O ₃	9038	0.67870
659.5385	5131.9	C ₄₅ H ₇₁ O ₃	9234	0.46086
673.5545	4308.2	C ₄₆ H ₇₃ O ₃	9430	0.23700
687.5703	4191.7	C ₄₇ H ₇₅ O ₃	9626	0.01566
701.5854	2133.1	C ₄₈ H ₇₇ O ₃	9823	0.80454
715.6014	3178.9	C ₄₉ H ₇₉ O ₃	10,019	0.58068
729.6165	3507.6	C ₅₀ H ₈₁ O ₃	10,215	0.36872
743.6323	3063.6	C ₅₁ H ₈₃ O ₃	10,411	0.14836

This plot can visually sort up to thousands of compounds horizontally according to the number of CH₂ groups and vertically according to class (heteroatom composition) and type (rings plus double bonds). Since these two classes have the same number of oxygen atoms, they have identical O/C ratios but distinguish themselves by different H/C ratios.

The attained results elucidate the transformation of oil components following irradiation. After irradiation with the xenon lamp (Suntest[®]), a slight shift of the peak to the higher masses appears in the recorded mass spectra, according to Griffiths et al. findings [31]. Therefore, it seems that a phenomenon of molecular polymerisation prevails on the destruction of the tri-, tetra- and penta-aromatic groups. Furthermore, since the increase in unsaturation correlates with the higher toxicity [44], our results could indicate higher toxicity for the oil after irradiation.

The plot of Figure 2 highlights the increase in the number of double bonds' rings as the KMD increases (*y*-axis) and the alkylation series along the *x*-axis. The solar irradiation causes a diminution of rings or double bonds (picks rarefaction in samples irradiated), a consequent Kendrick Nominal mass raising of 2 Da, and the Kendrick mass defect diminution. The irradiated crude oil sample shows an expansion of alkylation in compounds with a high degree of unsaturation and a reduced unsaturation number for molecules with a low alkylation degree.

Figure 3 shows the van Krevelen plot for the class of O₃ compounds found in the natural crude oil. The compounds in homologous series, corresponding to varying degrees of alkylation, appear along lines that intersect the value of 2 on the H/C axis. Similarly, a vertical line connects homologous series differing in degree of unsaturation. In agreement with the results in the Kendrick plot, most compounds have a low number of oxygen atoms and a high degree of unsaturation.

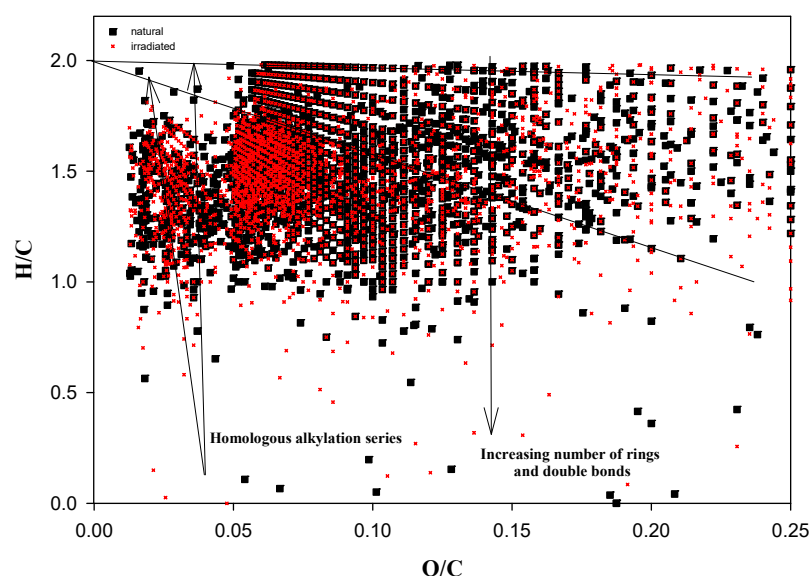


Figure 3. van Krevelen plot of the O_3 species found in natural (■) and irradiated oil (X). The compounds in homologous series, corresponding to varying degrees of alkylation, appear along lines that intersect the value of 2 on the H/C axis. Similarly, a vertical line connects homologous series differing in degree of unsaturation.

As the H/C ratio increases, the number of rings plus double bonds decreases. Thus, a slight shift to a lower H/C ratio (i.e., a higher number of rings plus double bonds) occurred. Figure 3 shows a minor shift of the data to the right due to increased oxidation and slight dehydration (the picks shift to the lower left) of hydrocarbons. Kendrick mass defect analysis has dramatically facilitated the interpretation of mass spectra, but it is still challenging to derive details for molecules that contribute to complex ultrahigh-resolution mass spectra.

Figure 4 shows the distribution of compounds associated with their number of oxygen atoms in natural and irradiated samples. In both samples, the number of total oxygenated compounds increases. The augmentation of oxygenated compounds should mainly refer to the O_3 and O_4 types present in the investigated model. The irradiation of crude oil in the solar simulator produces oil oxidation with a particular effect of double bonds oxygenation.

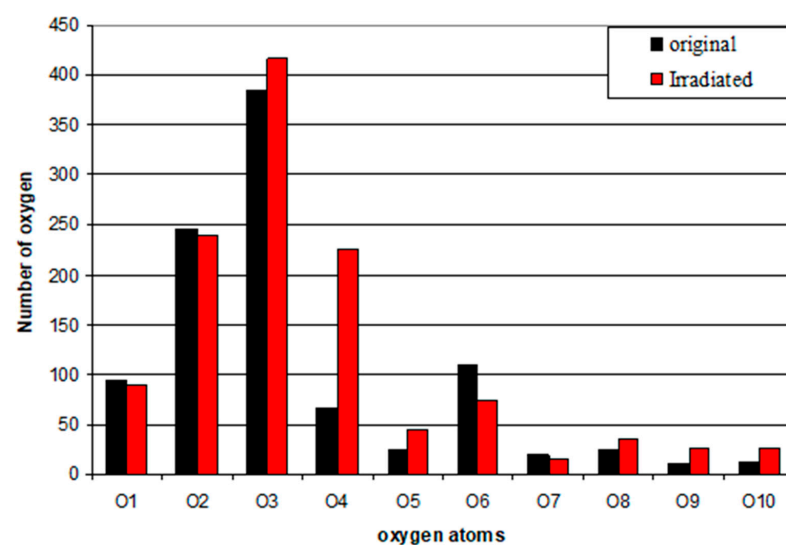


Figure 4. FT-ICR compositional analysis of natural and irradiated crude oil samples as a function of the number of oxygen atoms.

Figure 5 shows oxygen class Z-distributions for natural and irradiated samples, confirming a diminution of hydrogen deficiency index (~15–30% less) and augmentation of oxygen number after the light irradiation. Therefore, the light irradiation induces a manifest photo-oxidation of the crude oil composition. These results highlight toxicity as most of the new oxidised compounds are water-soluble, available in higher concentrations to the living organisms and probably more reactive and biologically active than their parent compounds [43,44].

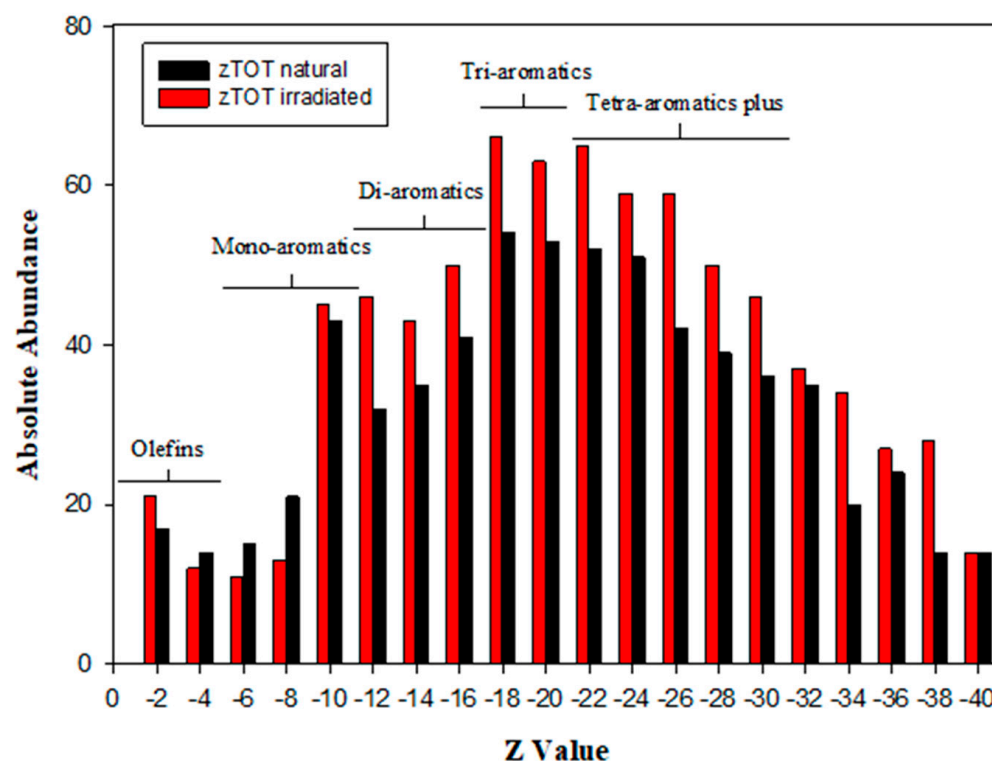


Figure 5. Oxygen class $\langle Z \rangle$-distributions for natural and irradiated samples.

2.2. Remediation of Oil-Polluted Water

Since crude oil lies over the surface of water and soil, it suffers solar irradiation. Solar degradation is one of the natural ways for petroleum decontamination, and, as a consequence, techniques based on light irradiation could be advantageous in the petroleum degradation processes. Enhanced light irradiation-based technologies are available, adopting different approaches for the scope [10–12,45].

The accidental dispersion of crude oil in water bodies forms a characteristic thin layer of not water-miscible compounds and a deeper layer of solubilised substances, which cannot easily separate from the aqueous solvent. In this direction, our approach was to prepare a water/oil suspension and investigate the efficiency of different cleaning methods. The water-soluble fraction of crude oil was undergone degradation by photocatalysis, sonolysis, and sonophotocatalysis, i.e., the simultaneous use of UV, titanium dioxide, and ultrasound emitter (UV + TiO₂ + US). GC-MS, liquid-state NMR, fluorescence, and high-resolution mass spectrometry (FT-ICR) analyses elucidated the chemical nature of water-soluble organic compounds after degradation processes and liquid-liquid extractions (LLEs). The results obtained in this study are concisely readable in Table 2.

Table 2. Synthetic results obtained from the different photodegradation processes of crude oil and oil water-soluble fraction (WSF) under investigation.

Degradation Method/System	GC-MS	¹ H-NMR	FT-ICR MS	Fluorescence
Photolysis (UV)/ Ageing of crude oil	- increase of C ₁₃ –C ₂₃ classes and a decrease of C ₇ –C ₁₂ types of compounds		- signal intensities increase-augmentation of compounds with a low molecular weight - a light increase of the number of oxygen atoms in the oxygenated species, in particular, O ₃ and O ₄ types - oxidation of crude oil with a particular effect on double bonds' oxygenation	
Photocatalysis (UV + TiO ₂)/ Oil Water-Soluble Fraction (WSF)	- increase of C ₅ compounds from 67% to 89% - decrease of C ₆ , C ₇ , C ₈ and C ₉ compounds - increase of branched alkanes from 50% to 65% - increase of cyclic alkanes from 4% to 5% - decrease of aromatic compounds from 23% to 13% - decrease of linear alkanes from 22% to 14%	- slight increase of linear and cyclic alkanes and a sharp decrease in aromatics - no other significant differences emerged in the composition of WSF before and after the processes	- a slight decrease in the total number of oxygenated compounds - the O ₁ and O ₂ classes prevailed over the other types	- aromatic compounds' decrease (about 46% after 1 h of treatment)
Sonolysis (US)/ Oil Water-Soluble Fraction (WSF)	- increase of C ₅ compounds from 67% to 91% - disappeared C ₉ class - increase of branched alkanes from 50% to 54% - increase of cyclic alkanes from 4% to 5% - increase of aromatic compounds from 23% to 24% - decrease of linear alkanes from 22% to 17%	- no significant differences emerged in the composition of treated and not treated WSF	- a low increase of oxygenated compounds: O ₁ , O ₂ and O ₇ classes and decrease of the other oxygenated types - a sharp increase in the number of compounds with a low molecular weight	- no significant differences emerged in the composition of aromatic compounds before and after the processes
Sonophotocatalysis (UV + TiO ₂ + US)/ Oil Water-Soluble Fraction (WSF)	- increase of C ₅ compounds from 67% to 91% - decrease C ₆ , C ₇ and C ₈ compounds; - disappeared C ₉ class - increase of branched alkanes from 50% to 64% - increase of cyclic alkanes from 4% to 9% - significant decrease of aromatic compounds from 23% to 7% - decrease of linear alkanes from 22% to 19%	- significant decrease of aromatic compounds from 23% to 7%	- the total number of oxygenated compounds decreased from 1203 to 993 - increase of compounds with low molecular weight and compounds with a low unsaturation degree	- aromatic compounds' decrease (about 48% after 1 h of treatment)

2.2.1. Photocatalytic Degradation

In the photocatalytic process, the water/oil suspension was treated for 1 h with UV irradiation in the presence of titanium dioxide. GC-MS analysis of WSF (Figure S3) evidenced increased C₅ compounds from 67% in not-treated WSF to 89% in the irradiated sample. Moreover, the amount of C₆, C₇, C₈, and C₉ compounds decreased. The analysis of chemical classes occurring in the irradiated WSF showed increased branched and cyclic

alkanes, from 50% to 65% (branched) and from 4% to 7% (cyclic), respectively. On the other hand, the number of linear alkanes underwent a slight decrease (from 22% to 14%), and the aromatic compounds had a sharp decline (from 23% to 13%).

$^1\text{H-NMR}$ spectra (Figures S4 and S5) confirmed a slight increase of linear and cyclic alkanes, and a sharp decrease in aromatics, as evidenced in the chromatographic analysis.

FT-ICR MS analysis showed a minor decrease in the total number of oxygenated compounds. The O_1 and O_2 classes prevailed over the other types (Figure 6).

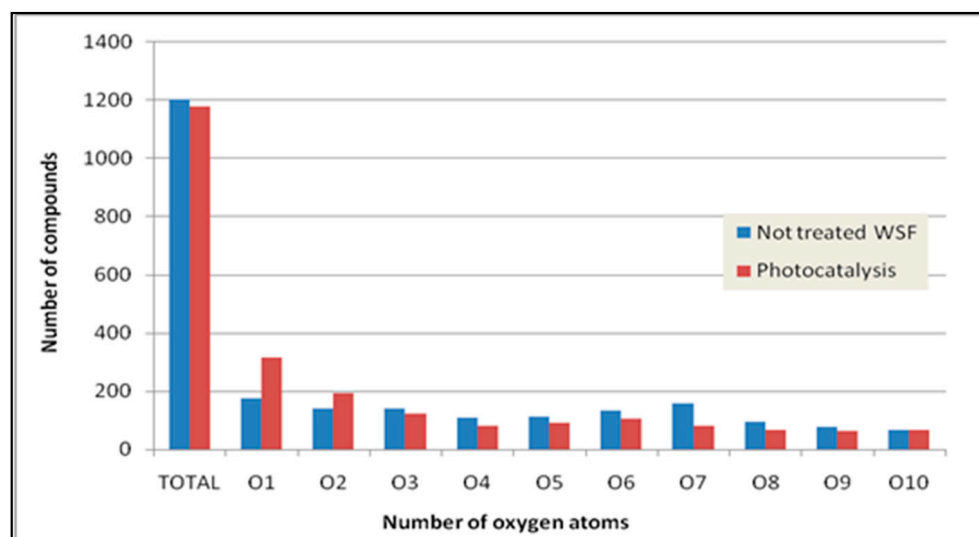


Figure 6. FT-ICR MS analysis of natural and 1-h photocatalysed WSF of crude oil as a function of the number of oxygen atoms.

Comparison of Kendrick plots constructed for the untreated sample (Figure 7a) and the photodegraded model (Figure 7b) shows an increase in the number of compounds with low molecular weight and low degree of unsaturation. The formation of several homologous series, with KDM values of 0.124, 0.137, 0.150, and so on, is underlined in the Kendrick diagram plotted for the treated sample. The unsaturation degree of these homologous series falls in the range $Z = -16$ to $Z = -20$.

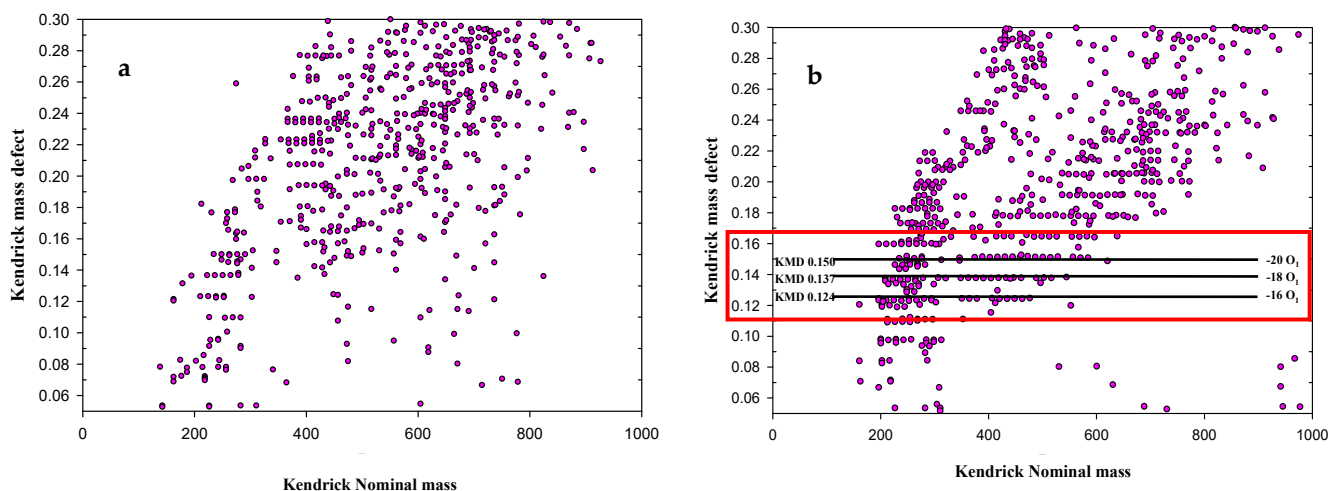


Figure 7. Kendrick mass plots of the O_1 - O_{10} species found in the untreated crude oil WSF (a) and the 1-h photocatalysed sample (b).

The van Krevelen diagram (Figure 8) shows an increase in O_1 class, reduced O/C ratio, and decreased unsaturated compounds in the treated sample compared to the untreated one. After photocatalysis, the number of compounds with a low number of oxygen atoms increased. As shown in Figure 6, the O_1 and O_2 classes prevailed over the other types, resulting in a decrease in the O/C ratio.

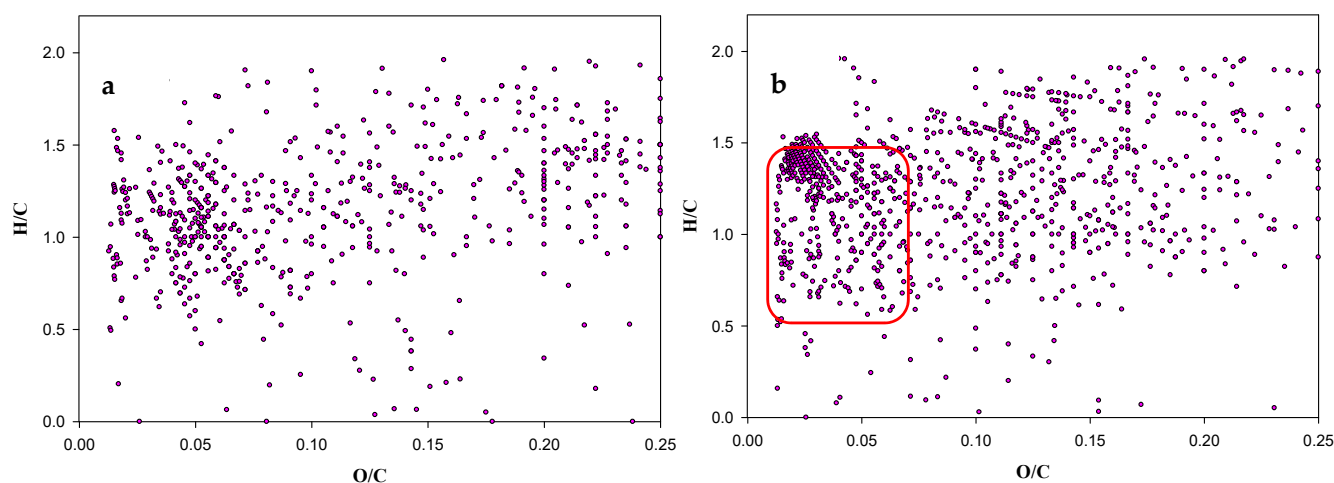


Figure 8. The van Krevelen plots of the O_1 – O_{10} species found in the untreated crude oil WSF (a) and the 1-h photocatalysed sample (b).

From fluorescence spectra (Figure S6), it was possible to argue aromatic compounds' decrease after 1-h photocatalytic treatment. Essentially, the absolute intensity of the peak at 347 nm decreases from 92.07 mAU for the natural sample to 49.50 mAU for the treated sample, with a reduction of 46%.

2.2.2. Ultrasonic Irradiation

In the sonolytic process, the water/oil suspension received 1-h ultrasound irradiation. GC-MS analysis (Figure S7) indicated that C_5 compounds increased from 67% to 91% at the end of sonolysis, evidencing a behaviour analogous to photocatalysis. Furthermore, the C_6 , C_7 and C_8 compounds decreased, similarly to the photocatalytic process; otherwise, the C_9 class disappeared. The analysis of functional groups evidenced that branched alkanes increased from 50% to 54% in the sonolysed WSF (from 50% to 65% in photocatalysis). Cyclic alkanes underwent a minor increase from 4% to 5% (like photocatalysis), but aromatic compounds slightly increased from 23% to 24% (decreased dramatically to 13% in photocatalysis). The number of linear alkanes decreased from 22% to 17% (22% to 14% in photocatalysis).

Liquid-state $^1\text{H-NMR}$ spectra (Figures S8 and S9) evidenced a relatively equal amount of the three classes of compounds in the not-treated and sonolysed samples. In conclusion, no significant differences emerged in the composition of WSF before and after the processes of sonication and photocatalysis, with a unique exception for aromatic compounds, as mentioned above in the case of photocatalysis.

From FTICR MS analysis, the total number of oxygenated compounds registered a low increase in the sonicated sample. O_1 , O_2 and O_7 classes increased, but the other oxygenated types decreased (Figure 9).

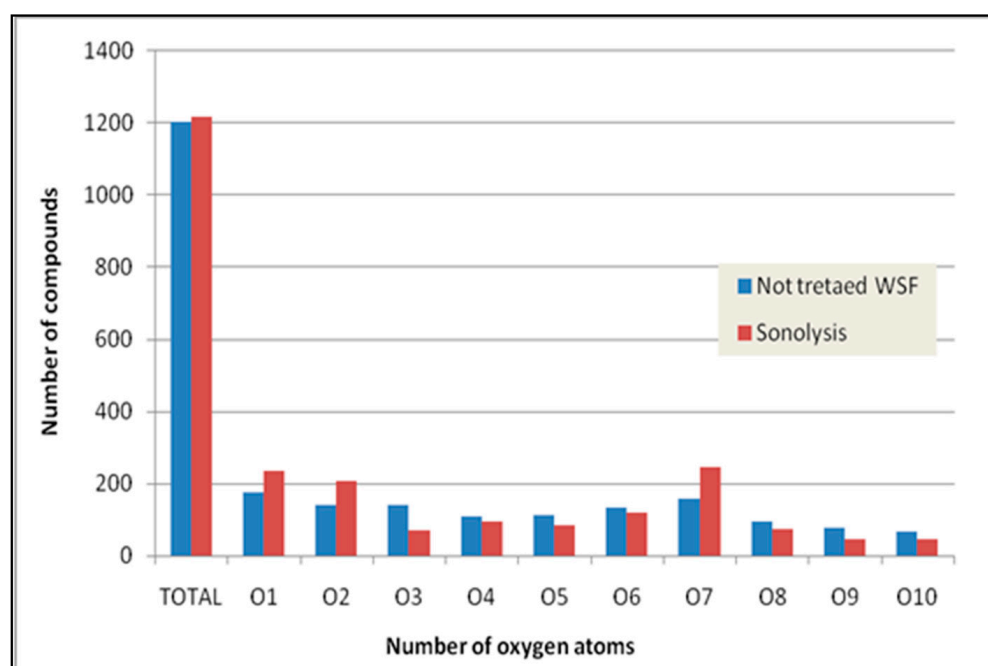


Figure 9. FT-ICR analysis of natural and 1-h sonicated WSF of crude oil samples as a function of the number of oxygen atoms.

Analysis of the Kendrick plot (Figure 10) after the degradation treatment shows a sharp increase in the number of compounds with low molecular weight. Seventy percent of compounds stay in the range m/z 159–597, and many homologous series with a high degree of unsaturation are visible.

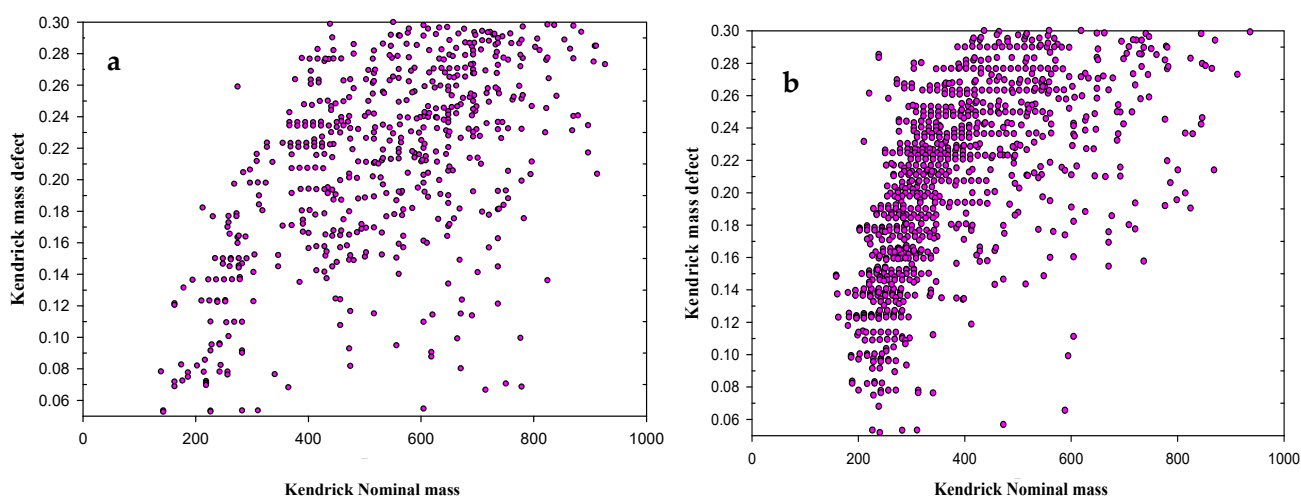


Figure 10. Kendrick mass plot of the O_1 – O_{10} species found in the not-treated WSF of crude oil (a) and after 1-h of US treatment (b).

The van Krevelen diagram (Figure 11) substantiates any differences between the natural and treated WSF samples.

The fluorescence study (Figure S10) confirms that the decrease of aromatic compounds is not so evident with US treatment. After 1-h of the sonolytic process, the absolute intensity of the maximum peak displays an insignificant drop from 99.96 mAU for the natural sample to 93.37 mAU for the treated one.

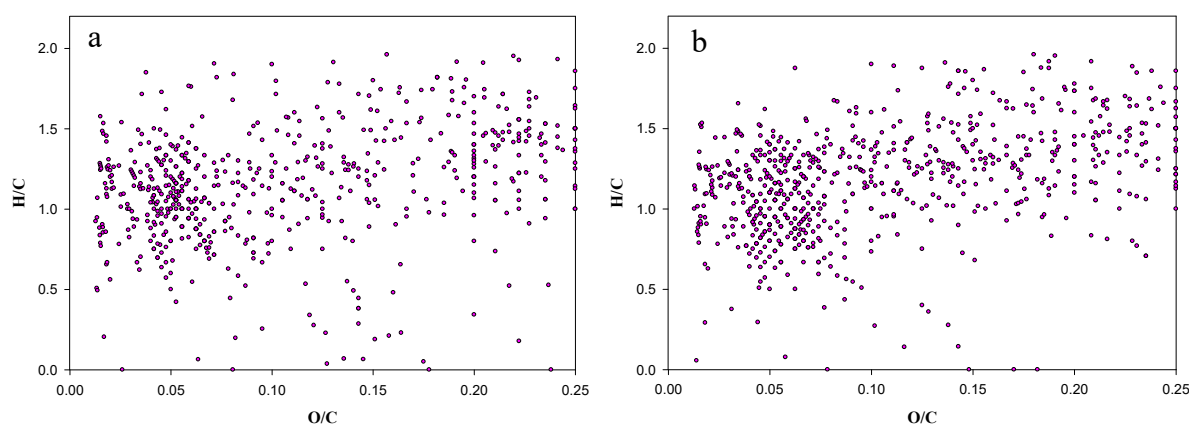


Figure 11. The van Krevelen plots of the O₁-O₁₀ species found in the not-treated WSF of crude oil (a) and after 1-h US treatment (b).

2.2.3. Sonophotocatalytic Degradation

The contemporary use of UV irradiation, titanium dioxide and ultrasound irradiation to treat the oil aqueous suspension shows results mainly similar to those obtained with sonolysis or photocatalysis.

GC-MS analysis (Figure S11) demonstrated that after 1-h of treatment, C₅ compounds increased from 67% in not-treated WSF to 91% in the treated sample, while C₆, C₇ and C₈ compounds decreased; C₉ compounds were not detected (like the simple US). The analysis of functional groups in the sonophotocatalytic degradation evidenced an increase from 50% to 64% of branched alkanes (similar to photocatalysis) and from 4% to 9% of cyclic alkanes (higher than the other technologies). The number of linear alkanes underwent a slight decrease (from 22% to 19%, similar to the other technologies). In comparison, aromatic compounds showed the sharpest decline (from 23% to 7%), also proved by integrating NMR spectra (Figures S12 and S13). In the natural WSF, the aromatics alkanes occupied 19% of the whole spectral area, whilst in the treated sample, this amount decreases up to 3.3%. On the other hand, the amount of linear and cyclic alkanes increases by about 7–8%.

Figure 12 shows the trend of oxygenated compounds after sonophotocatalytic treatment. In this case, the total number of oxygenated compounds decreased from 1203 (not treated WSF) to 993 (treated WSF).

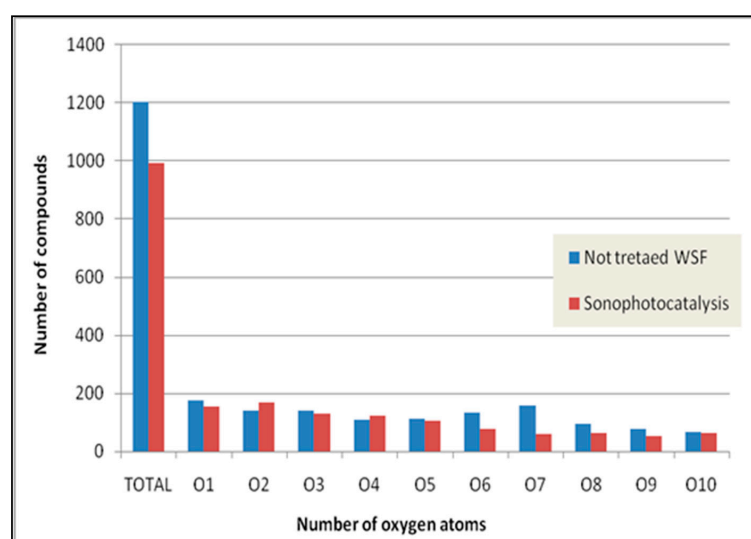


Figure 12. FT-ICR MS analysis of natural and 1-h sonophotocatalysed WSF sample of crude oil as a function of the number of oxygen atoms.

Comparison of Kendrick plots (Figure 13) obtained for the not-treated and treated samples showed an increased number of compounds with low molecular weight, especially in the range m/z 169–369, and compounds with a low unsaturation degree.

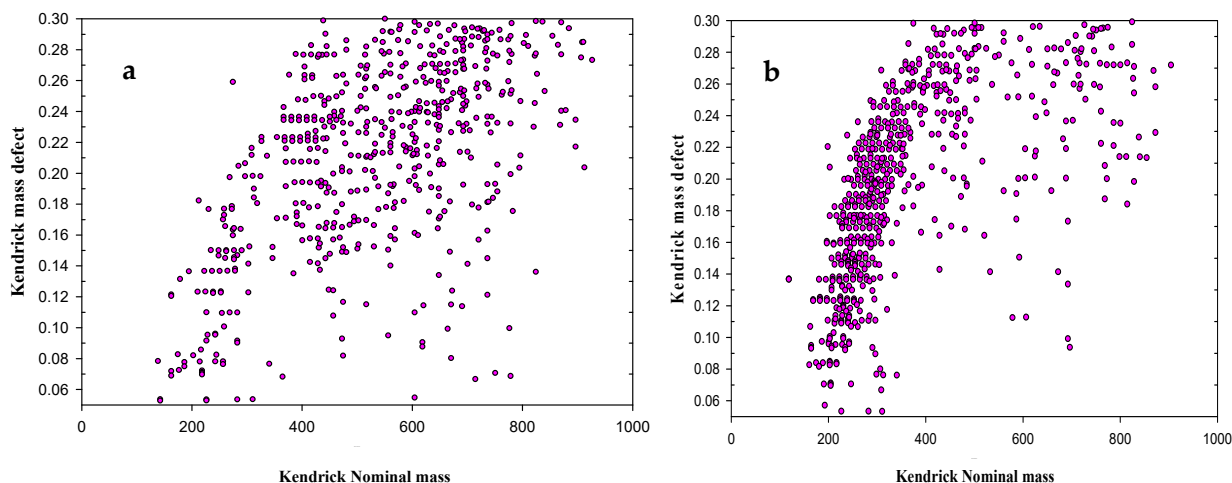


Figure 13. Kendrick mass plots of the O_1 - O_{10} species found in the not-treated WSF of crude oil (a) and after 1-h of sonophotocatalytic treatment (b).

The van Krevelen diagram (Figure 14) let us see an intensification of signals relative to oxygenated compounds with an O/C ratio in the range 0.10–0.25.

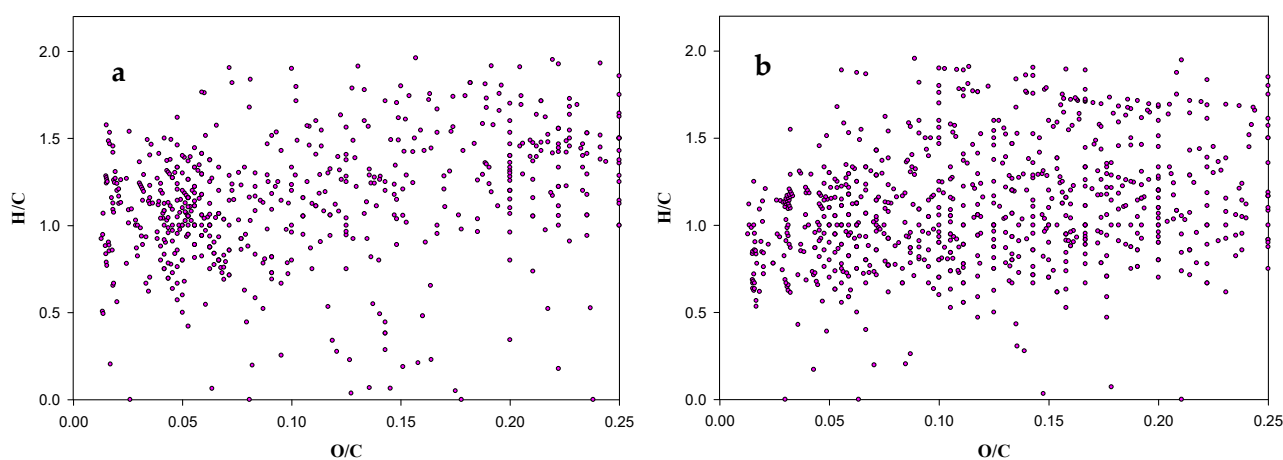


Figure 14. The van Krevelen plots of the O_1 - O_{10} species found in the not-treated WSF of crude oil (a) and after 1-h of sonophotocatalytic treatment (b).

Fluorescence spectra (Figure S14) substantiated the decreasing of aromatic compounds after 1-h sonophotocatalytic treatment. The absolute intensity of the peak at 347 nm decreased from 89.92 mAU for the natural sample to 47.95 mAU for the treated sample, reducing by 48%.

3. Materials and Methods

3.1. Crude Oil and Chemicals

The director of the Eni-Cova Oil Plant in Val d'Agri (Basilicata Region, Southern Italy) kindly provided the oil sample taken from the first step of oil purification after extraction, including dehydration and degasification. Table 3 accounts for the elemental composition reported in the label accompanying the sample delivered for this research.

Table 3. Elemental composition (%) of the oil sample taken from the first step of oil purification after extraction, including dehydration and degasification ^a.

C	H	N	O ^b	S
85.4 ± 2.8	11.8 ± 1.4	0.3 ± 0.1	0.6 ± 0.4	1.9 ± 0.9

^a Metals (Ni and V) < 1000 ppm. ^b Obtained as the complement to 100.

All chemicals used were of analytical grade. TiO₂ Degussa P-25, obtained as a gift from Evonik (Hanau, Germany), was the catalyst adopted. Table 4 reports a summary scheme of the investigation executed.

Table 4. Experiments performed and analytical methods used in this study.

Experiments Performed	Treated System	Analytical Methods Applied			
		GC-MS	¹ H-NMR	FT-ICR MS	Fluorescence
Artificial ageing process by photolysis (UV)	Crude oil	X		X	
Remediation process by photocatalysis (UV + TiO ₂)	Oil WSF	X	X	X	X
Remediation process by sonolysis (US)	Oil WSF	X	X	X	X
Remediation process by sonophotocatalysis (UV + TiO ₂ + US)	Oil WSF	X	X	X	X

3.2. Photodegradation Apparatus

The Suntest CPS+ (Heraeus Industrietechnik GmbH, Hanau, Germany), equipped with a xenon lamp of 1.1 kW, protected employing a quartz plate (total passing wavelength: 300 nm < λ < 800 nm), was the solar simulator adopted for photochemical reactions. The temperature of the irradiation chamber was 25 °C, maintained through both a thermostatic bath and a conditioned airflow. During the experiments, the crude oil samples were kept up in the horizontal position, creating a homogeneous film of 0.5 cm thickness.

3.3. Photodegradation Process and Sample Preparation for ESI FT-ICR MS

The protocol used for oil ageing experiments was: (i) the irradiation of the natural crude oil (10 mL) for a week in the borosilicate planar reactor; (ii) crude oil samples preparation by dissolving ~30 mg of material in 30 mL of toluene; (iii) withdrawal of 1 mL solution and its dilution with 0.5 mL methanol; addition of either 10 µL acetic acid (for positive ion ESI) or 10 µL ammonium hydroxide (for negative ion ESI) to facilitate protonation or deprotonation in the electrospray ionisation process, respectively.

3.4. Ultrasonic Irradiation of WSF Samples

A crude oil/water suspension was arranged in a borosilicate decanter (5 L) equipped with a Teflon tap at the bottom. The decanter was filled with 3.5 L of ultrapure water; the crude oil was added at the ratio of 1/20 (oil/water), and the suspension was magnetically stirred and then kept in the dark for 30 days at constant temperature (25 °C) to reach equilibrium and the separation of oil phase on the surface of the aqueous phase. Aqueous samples were drawn off through the Teflon tap without disturbing the oil/water separation surface. The collected aqueous sample (500 mL) underwent cotton filtration, to avoid the formation of an emulsion in the solution. The ultrasonic degradation tool was the immersible ultrasonic emitter Sinaptec Nexus P198-R (Sinaptec, Lezennes, France), an

ultrasonic module furnished with a titanium sonotrode (S23-10-1/2, Sinaptec), an electrical signal of frequency close to 20 kHz, and a voltage of about 1 kV. In this configuration, the electric power provided by the generator (Nexus P198-R, same manufacturer) is adjustable between 7 W and 100 W, as indicated on a digital display panel. However, this electrical measurement does not determine with high precision the acoustic power dissipated in the liquid. The experimental temperature was fixed to 25 °C.

3.5. Photocatalytic and Sonophotocatalytic Degradation of WSF Samples

The photocatalytic method to degrade the water-soluble fraction of crude oil utilises a 125 W high-pressure mercury lamp (Philips-HPK, Philips, Turnhout, Belgium) that provides its maximum energy at 365 nm, with a range of emission from 195 to 580 nm. The catalyst was TiO₂ (80% anatase–20% rutile). The simultaneous use of the mercury lamp, titanium dioxide and the ultrasound emitter (UV + TiO₂ + US) permitted the sonophotocatalytic degradation. The experimental temperature was 25 °C for photocatalysis and sonophotocatalysis trials.

3.6. Liquid–Liquid Extraction (LLE)

The experimental protocol was (i) to collect samples of the oil WSF after 15, 30, 45, and 60 min of treatment; (ii) to extract in triplicate 30 mL of each sample in a separatory funnel (50 mL) with 3 mL dichloromethane for GC-MS analysis and (iii) another 30 mL with the same solvent for ¹H-NMR spectroscopy; (iv) to perform fluorescence analysis using 5 mL of the aqueous solution without extraction.

The internal standard used for assessing the reproducibility of WSF extraction was 1 mL of 1,3-dibromopropane (26.7 mg L⁻¹) added to the volume of dichloromethane needed for each liquid–liquid extraction. In addition, it was necessary to add 1.0 mL of 1-bromododecane (29.0 mg L⁻¹) to evaluate the GC-MS analysis reproducibility at the end of each extraction. Thus, the injection volume was 1 µL extract for each GC-MS run.

3.7. Analysis of Fluorescence

A research-grade spectrofluorometer FP-6500 Jasco (Jasco Corporation, Cremella, Italy) was available for fluorescence analysis. This analysis was necessary to appreciate the aromatic compounds remaining in the water-soluble fraction of crude oil. The spectrofluorometer FP-6500 Jasco, adopting as emitting source a DC-powered 150 W xenon lamp (in a sealed housing), employs a photometric rationing system, which utilises a second photomultiplier tube to monitor and compensate for any variations in the intensity of the xenon source, thus ensuring maximum analytical stability. Furthermore, a concave holographic grating monochromator with optimised blaze angles provides maximum sensitivity over the entire wavelength range; (220–750 nm; 1 nm resolution).

The fluorescence optical path adopted was 1 cm in quartz cells (volume ca 5 cm³) at 237 and 320 nm excitation and 347 and 360 nm emission.

3.8. ¹H-NMR Analysis

A Varian Oxford AS400 spectrometer (Palo Alto, CA, USA), operating at 400 MHz, was enough for the ¹H-NMR spectra recording. The set temperature for the used 5 mm non-gradient broadband inverse (BBI) probe was 25 °C.

All the ¹H-NMR spectra have tetramethylsilane (TMS) as reference under the acquisition parameters shown in Table 5.

In degradation experiments, liquid–liquid extraction with chloroform permitted to isolate the water-soluble fraction of crude oil. After the complete evaporation of the solvent in a rotary evaporator, the addition of 500 µL deuterated chloroform (CDCl₃) permitted to recuperate the residual organic mixture.

Table 5. $^1\text{H-NMR}$ acquisition parameters.

Instrument	Solvent	Acquisition Time	Spectral Width	Line Broadening	Number of Scans
Varian Oxford AS400	CDCl_3	2.049 s	6410.3 Hz	0.20 Hz	512

3.9. Mass Spectrometry of Polar Components

The instrument available to determine polar components was the micro ESI/FT-ICR/MS 7 T Thermo Electron (Waltham, MA, USA).

The method used for the routine analyses permitted a mass accuracy better than 2 ppm by external calibration, using the mixture of caffeine, MRFA, and Ultramark. The technique separated more than 6000 ion signals belonging to chemically different elemental compositions with a 200,000 resolving power ($m/\Delta m_{50\%}$ at m/z 400) in positive electrospray mode. The robustness of this equipment, combined with unprecedented ease of use, ultra-high mass accuracy, high sensitivity, and excellent resolving power, make it an ideal instrument for analysis. The infusion of the samples at a flow rate of 5 $\mu\text{L}/\text{min}$ permitted the best result in terms of spectrum resolution. ESI conditions were: needle voltage, +4.5 kV; heated capillary current 4 A; tube lens voltage 135.12; temperature 300 $^\circ\text{C}$; N_2 speed 2.33 u.a.; aux gas flow rate 0.73; scansions per second 1000.

4. Conclusions

In this study, we tried to characterise the ageing process of crude oil simulating solar irradiation on a thin layer of an oil sample. As a result, FT-ICR MS evidenced an augmentation of compounds with low molecular weight and a slight increase of the number of oxygen atoms in the oxygenated species, as depicted in Kendrick and van Krevelen diagrams. Furthermore, the simulated ageing produced the oxidation of crude oil with a particular effect on double bonds' oxygenation, as confirmed by the disappearance of alkenes in gas chromatographic analysis. The observed results seem to be recognisable because the energy irradiated with the xenon lamp could be enough for catalysing the reaction of olefins with the atmospheric oxygen following a bridge mechanism.

We experimented with different solutions for the cleaning treatment of oil-polluted water (photocatalysis, sonolysis, and sonophotocatalysis). GC-MS analyses of the water-soluble fraction of crude oil for both natural and treated samples discovered that only a few compounds are detectable in the aqueous solution, principally C_5 -organic chains (~50%). Low amounts of C_6 , C_7 , C_8 and C_9 chains were also present. Both GC-MS and liquid state $^1\text{H-NMR}$ signals showed that the branched alkanes were the principal chemical class in the soluble fraction of oil, followed by a small amount of linear and aromatic alkanes.

With all the degradation methods utilised, an increase of the C_5 -class and a decrease of C_6 – C_9 types of compounds was evident. Furthermore, the FT-ICR comparative analyses of oxygenated species elucidated that the total number of O-compounds in the treated WSF samples is different for all of the degradation methods experimented. The number of the oxygenated compounds slightly decreased with photocatalysis compared to the non-treated sample. An opposite trend appeared with the sonolysis treatment. The sonophotocatalytic method showed a sharp reduction in the number of oxygenated compounds, probably due to the volatilisation of small molecules formed during the oxidation process. It is conceivable that ultrasound can promote this volatilisation. The degradation of the water-soluble fraction of crude oil performed with photocatalysis and sonophotocatalysis led to an apparent decrease of aromatic compounds of 46% and 48%, respectively, for the two techniques, as also confirmed by the fluorescence analysis. With the use of sonolysis, there was no effect on the number of aromatic compounds. Nevertheless, all the degradation methods applied were capable of increasing the number of cyclic alkanes. Therefore, we could speculate that ultrasound in sonophotocatalytic technology can affect the rate of the

photocatalytic degradation of the organic pollutants due to a synergistic effect typically observed with an increase of the degradation process efficiency.

In conclusion, our results confirm the photo-oxidation effect caused by light irradiation either on crude oil (simulated ageing) or on the soluble oil fraction. Naturally, the behaviour of each oil type could be different, and then it is not possible to generalise our findings to all cases of oil spilling and environmental remediation. Therefore, it is necessary to check case by case before reaching specific solutions for more efficient remediation processes to avoid making the situation worse.

Supplementary Materials: The following are available online at <https://www.mdpi.com/article/10.3390/catal11080954/s1> Figure S1: Percentage of compounds in crude oil as recognized by GC-MS (blue column) and $^1\text{H-NMR}$ (red column). Figure S2: GC-MS compositional analysis of crude oil (blue column) and solar simulator irradiated crude oil (red column), as a function of the number of carbon atoms (A); composition of crude oil as a function of the type of compounds, LH: linear aliphatic hydrocarbons; BH: branched aliphatic hydrocarbons; CH: cyclic aliphatic hydrocarbons; AH: aromatic hydrocarbons; AL: alkenes (B); composition of the linear aliphatic hydrocarbons as a function of the number of carbon atoms (C); composition of the branched aliphatic hydrocarbons fraction as a function of the number of carbon atoms (D); composition of the cyclic hydrocarbons as a function of the number of carbon atoms (E); composition of the aromatic hydrocarbons fraction as a function of the number of carbon atoms (F). Figure S3: GC-MS compositional analysis of WSF crude oil before (red column) and after (blue column) photocatalysis: distribution of hydrocarbons as a function of the number of carbon atoms (A) and distribution of the compounds as a function of chemical species (B). Figure S4: $^1\text{H-NMR}$ spectra of WSF crude oil before (A) and after (B) photocatalysis. Figure S5: $^1\text{H-NMR}$ compositional analysis of WSF crude oil before (red column) and after (blue column) photocatalysis: distribution of the compounds as a function of chemical species. Figure S6: Fluorescence spectra of WSF crude oil before (blue line) and after (red line) photocatalysis. Figure S7: GC-MS compositional analysis of WSF crude oil before (red column) and after (blue column) sonolysis: distribution of hydrocarbons as a function of the number of carbon atoms (A) and distribution of the compounds as a function of chemical species (B). Figure S8: $^1\text{H-NMR}$ spectra of WSF crude oil before (A) and after (B) sonolysis. Figure S9: $^1\text{H-NMR}$ compositional analysis of WSF crude oil before (red column) and after (blue column) sonolysis: distribution of the compounds as a function of chemical species. Figure S10: Fluorescence spectra of WSF crude oil before (blue line) and after (red line) sonolysis. Figure S11: GC-MS compositional analysis of WSF crude oil before (red column) and after (blue column) sonophotocatalysis: distribution of hydrocarbons as a function of the number of carbon atoms (A) and distribution of the compounds as a function of chemical species (B). Figure S12: $^1\text{H-NMR}$ spectra of WSF crude oil before (A) and after (B) sonophotocatalysis. Figure S13: $^1\text{H-NMR}$ compositional analysis of WSF crude oil before (red column) and after (blue column) sonophotocatalysis: distribution of the compounds as a function of chemical species. Figure S14: Fluorescence spectra of WSF crude oil before (blue line) and after (red line) sonophotocatalysis.

Author Contributions: Conceptualisation, F.L., S.A.B. and L.S.; Data curation, F.L., G.B. and S.A.B.; Formal analysis, L.S.; Investigation, L.S.; Methodology, G.B.; Resources, S.A.B.; Writing—original draft, F.L. and L.S.; Writing—review and editing, S.A.B. All authors have read and agreed to the published version of the manuscript.

Funding: This research received no external funding.

Data Availability Statement: Data supporting results reported in this paper can be found at the Department of Sciences, University of Basilicata, Via dell'Ateneo Lucano 10, 85100, Potenza, Italy. Due to the multitude of files produced for this investigation, a link will be provided under specific requests.

Acknowledgments: We acknowledge the Director of ENI-COVA Oil Plant in Val d'Agri (Basilicata Region, Southern Italy), who kindly provided the oil sample. Special thanks go to Mauro Tummolo, and to Jean-Marc Chovelon, University Claud Bernard Lyon 1, for the sonolysis and sonophotocatalysis data.

Conflicts of Interest: The authors declare no conflict of interest.

References

1. Richard Parent. Available online: <https://www.experts.com/articles/toxicity-of-crude-oil-and-its-vapors-by-richard-parent> (accessed on 17 April 2020).
2. McKee, R.H.; White, R. The Mammalian Toxicological Hazards of Petroleum-Derived Substances: An Overview of the Petroleum Industry Response to the High Production Volume Challenge Program. *Int. J. Toxicol.* **2014**, *33* (Suppl. 1), 4S–16S. [CrossRef]
3. Laffon, B.; Pásaro, E.; Valdiglesias, V. Effects of exposure to oil spills on human health: Updated review. *J. Toxicol. Environ. Health Part B* **2016**, *19*, 105–128. [CrossRef] [PubMed]
4. Guarino, C.; Spada, V.; Sciarrillo, R. Assessment of three approaches of bioremediation (Natural Attenuation, Landfarming and Bioaugmentation–Assisted Landfarming) for a petroleum hydrocarbons contaminated soil. *Chemosphere* **2017**, *170*, 10–16. [CrossRef]
5. Cheng, Y.; Wang, L.; Faustorilla, V.; Megharaj, M.; Naidu, R.; Chen, Z. Integrated electrochemical treatment systems for facilitating the bioremediation of oil spill contaminated soil. *Chemosphere* **2017**, *175*, 294–299. [CrossRef] [PubMed]
6. Safdari, M.-S.; Kariminia, H.-R.; Rahmati, M.; Fazlollahi, F.; Polasko, A.; Mahendra, S.; Wilding, W.V.; Fletcher, T.H. Development of bioreactors for comparative study of natural attenuation, biostimulation, and bioaugmentation of petroleum-hydrocarbon contaminated soil. *J. Hazard. Mater.* **2018**, *342*, 270–278. [CrossRef] [PubMed]
7. Bao, M.T.; Wang, L.N.; Sun, P.Y.; Cao, L.X.; Zou, J.; Li, Y.M. Biodegradation of crude oil using an efficient microbial consortium in a simulated marine environment. *Mar. Pollut. Bull.* **2012**, *64*, 1177–1185. [CrossRef]
8. Adzighli, L.; Bacosa, H.P.; Deng, Y. Response of microbial communities to oil spill in the Gulf of Mexico: A review. *Afr. J. Microbiol. Res.* **2018**, *12*, 536–545. [CrossRef]
9. Al-Gharabally, D.; Al-Barood, A. Kuwait environmental remediation program (KERP): Remediation demonstration strategy. *Biol. Chem. Res.* **2015**, *2015*, 289–296. Available online: <http://www.ss-pub.org/wp-content/uploads/2015/09/BCR2015051501.pdf> (accessed on 12 September 2020).
10. Shankar, R.; Won, J.-S.; An, J.-G.; Yim, U.-H. A practical review on photooxidation of crude oil: Laboratory lamp setup and factors affecting it. *Water Res.* **2015**, *68*, 304–315. [CrossRef]
11. Ray, P.Z.; Chen, H.; Podgorski, D.C.; McKenna, A.M.; Tarr, M.A. Sunlight creates oxygenated species in water-soluble fractions of deep water horizon oil. *J. Hazard. Mater.* **2014**, *280*, 636–643. [CrossRef]
12. Vaughan, P.P.; Wilson, T.; Kamerman, R.; Hagy, M.E.; McKenna, A.; Chen, H.; Jeffrey, W.H. Photochemical changes in water accommodated fractions of MC252 and surrogate oil created during solar exposure as determined by FT-ICR MS. *Mar. Pollut. Bull.* **2016**, *104*, 262–268. [CrossRef]
13. Lee, K.; Boufadel, M.; Chen, B.; Foght, J.; Hodson, P.; Swanson, S.; Venosa, A. *Expert Panel Report on the Behaviour and Environmental Impacts of Crude Oil Released into Aqueous Environments*; Royal Society of Canada: Ottawa, ON, Canada, 2015; pp. 38–415. ISBN 978-1-928140-02-3. Available online: https://www.rsc-src.ca/sites/default/files/OIW%20Report_1.pdf. (accessed on 12 September 2020).
14. Cho, E.; Park, M.; Hur, M.; Kang, G.; Kim, Y.H.; Kim, S. Molecular-level investigation of soils contaminated by oil spilled during the Gulf War. *J. Hazard. Mater.* **2019**, *373*, 271–277. [CrossRef] [PubMed]
15. Islam, A.; Cho, Y.; Yim, U.H.; Shim, W.J.; Kim, Y.H.; Kim, S. The comparison of naturally weathered oil and artificially photo-degraded oil at the molecular level by a combination of SARA fractionation and FT-ICR MS. *J. Hazard. Mater.* **2013**, *263*, 404–411. [CrossRef]
16. Lelario, F.; Brienza, M.; Bufo, S.A.; Scrano, L. Effectiveness of different advanced oxidation processes (AOPs) on the abatement of the model compound mepanipyrin in water. *J. Photochem. Photobiol. A Chem.* **2016**, *321*, 187–201. [CrossRef]
17. Hall, G.J.; Frysiner, G.S.; Aeppli, C.; Carmichael, C.A.; Gros, J.; Lemkau, K.L.; Nelson, R.K.; Reddy, C.M. Oxygenated weathering products of Deepwater Horizon oil come from surprising precursors. *Mar. Pollut. Bull.* **2013**, *75*, 140–149. [CrossRef] [PubMed]
18. Prince, R.C.; McFarlin, K.M.; Butler, J.D.; Febbo, E.J.; Wang, F.C.; Nedwed, T.J. The primary biodegradation of dispersed crude oil in the sea. *Chemosphere* **2013**, *90*, 521–526. [CrossRef] [PubMed]
19. Gros, J.; Reddy, C.M.; Aeppli, C.; Nelson, R.K.; Carmichael, C.A.; Arey, J.S. Resolving biodegradation patterns of persistent saturated hydrocarbons in weathered oil samples from the Deepwater Horizon disaster. *Environ. Sci. Technol.* **2014**, *48*, 1628–1637. [CrossRef]
20. Seidel, M.; Kleindienst, S.; Dittmar, T.; Joye, S.B.; Medeiros, P.M. Biodegradation of crude oil and dispersants in deep seawater from the Gulf of Mexico: Insights from ultra-high resolution mass spectrometry. *Deep Sea Res. Part II Top. Stud. Oceanogr.* **2016**, *129*, 108–118. [CrossRef]
21. Bacosa, H.P.; Erdner, D.L.; Liu, Z. Differentiating the roles of photooxidation and biodegradation in the weathering of Light Louisiana Sweet crude oil in surface water from the Deepwater Horizon site. *Mar. Pollut. Bull.* **2015**, *95*, 265–272. [CrossRef] [PubMed]
22. Barrow, M.P.; Peru, K.M.; Fahlman, B.; Hewitt, L.M.; Frank, R.A.; Headley, J.V. Beyond naphthenic acids: Environmental screening of water from natural sources and the Athabasca oil sands industry using atmospheric pressure photoionisation Fourier transform ion cyclotron resonance mass spectrometry. *J. Am. Soc. Mass Spectrom.* **2015**, *26*, 1508–1521. [CrossRef]
23. D’Auria, M.; Racioppi, R.; Velluzzi, V. Photodegradation of crude oil: Liquid injection and headspace solid-phase microextraction for crude oil analysis by gas chromatography with mass spectrometer detector. *J. Chromatogr. Sci.* **2008**, *46*, 339–344. [CrossRef]

24. D’Auria, M.; Emanuele, L.; Racioppi, R.; Velluzzi, V. Photochemical degradation of crude oil: Comparison between direct irradiation, photocatalysis, and photocatalysis on zeolite. *J. Hazard. Mater.* **2009**, *164*, 32–38. [[CrossRef](#)]
25. Kim, D.; Ha, S.Y.; An, J.G.; Cha, S.; Yim, U.H.; Kim, S. Estimating degree of degradation of spilled oils based on relative abundance of aromatic compounds observed by paper spray ionisation mass spectrometry. *J. Hazard. Mater.* **2018**, *359*, 421–428. [[CrossRef](#)] [[PubMed](#)]
26. Christopher, M.R.; Quinn, J.G. GC-MS analysis of total petroleum hydrocarbons and polycyclic aromatic hydrocarbons in seawater samples after the North Cape oil spill. *Mar. Pollut. Bull.* **1999**, *38*, 126–135. [[CrossRef](#)]
27. de Oteyza, T.G.; Grimalt, J.O. GC and GC-MS characterisation of crude oil transformation in sediments and microbial mat samples after the 1991 oil spill in the Saudi Arabian Gulf coast. *Environ. Pollut.* **2006**, *139*, 523–531. [[CrossRef](#)] [[PubMed](#)]
28. Gonzalez, J.J.; Vinas, L.; Franco, M.A.; Fumega, J.; Soriano, J.A.; Grueiro, G.; Muniategui, S.; Lopez-Mahia, P.; Prada, D.; Bayona, J.M.; et al. Spatial and temporal distribution of dissolved/dispersed aromatic hydrocarbons in seawater in the area affected by the Prestige oil spill. *Mar. Pollut. Bull.* **2006**, *53*, 250–259. [[CrossRef](#)]
29. McKenna, A.M.; Nelson, R.K.; Reddy, C.M.; Savory, J.J.; Kaiser, N.K.; Fitzsimmons, J.E.; Marshall, A.G.; Rodgers, R.P. Expansion of the analytical window for oil spill characterisation by ultrahigh resolution mass spectrometry: Beyond gas chromatography. *Environ. Sci. Technol.* **2013**, *47*, 7530–7539. [[CrossRef](#)] [[PubMed](#)]
30. Haleyr, N.; Shahsavari, E.; Mansur, A.A.; Koshlaf, E.; Morrison, P.D.; Osborn, A.M.; Ball, A.S. Comparison of rapid solvent extraction systems for the GC-MS/MS characterisation of polycyclic aromatic hydrocarbons in aged, contaminated soil. *MethodsX* **2016**, *3*, 364–370. [[CrossRef](#)] [[PubMed](#)]
31. Oldenburg, T.B.; Jones, M.; Huang, H.; Bennett, B.; Shafiee, N.S.; Head, I.; Larter, S.R. The controls on the composition of biodegraded oils in the deep subsurface—Part 4. Destruction and production of high molecular weight non-hydrocarbon species and destruction of aromatic hydrocarbons during progressive in-reservoir biodegradation. *Org. Geochem.* **2017**, *114*, 57–80. [[CrossRef](#)]
32. Griffiths, M.T.; Da Campo, R.; O’Connor, P.B.; Barrow, M.P. Throwing light on petroleum: Simulated exposure of crude oil to sunlight and characterisation using atmospheric pressure photoionisation Fourier transform ion cyclotron resonance mass spectrometry. *Anal. Chem.* **2013**, *86*, 527–534. [[CrossRef](#)]
33. Lemkau, K.L.; McKenna, A.M.; Podgorski, D.C.; Rodgers, R.P.; Reddy, C.M. Molecular evidence of heavy-oil weathering following the M/V Cosco Busan spill: Insights from Fourier transform ion cyclotron resonance mass spectrometry. *Environ. Sci. Technol.* **2014**, *48*, 3760–3767. [[CrossRef](#)]
34. Marshall, A.G.; Rodgers, R.P. Petroleomics: The Next Grand Challenge for Chemical Analysis. *Acc. Chem. Res.* **2004**, *37*, 53–59. [[CrossRef](#)]
35. Kendrick, E. A Mass Scale Based on $\text{CH}_2=14.0000$ for High Resolution Mass Spectrometry of Organic Compounds. *Anal. Chem.* **1963**, *35*, 2146–2154. [[CrossRef](#)]
36. Hughey, C.A.; Hendrickson, C.L.; Rodgers, R.P.; Marshall, A.G.; Qian, K. Kendrick mass defect spectroscopy: A compact visual analysis for ultrahigh-resolution broadband mass spectra. *Anal. Chem.* **2001**, *73*, 4676–4681. [[CrossRef](#)] [[PubMed](#)]
37. Hughey, C.A.; Rodgers, R.P.; Marshall, A.G. Resolution of 11,000 compositionally distinct components in a single electrospray ionisation Fourier transform ion cyclotron resonance mass spectrum of crude oil. *Anal. Chem.* **2002**, *74*, 4145–4149. [[CrossRef](#)]
38. van Krevelen, D.W. Graphical-statistical method for the study of structure and reaction processes of coal. *Fuel* **1950**, *29*, 269–284.
39. Kim, S.; Kramer, R.W.; Hatcher, P.G. Graphical method for analysis of ultrahigh-resolution broadband mass spectra of natural organic matter, the van Krevelen diagram. *Anal. Chem.* **2003**, *75*, 5336–5344. [[CrossRef](#)]
40. Hughey, C.A.; Rodgers, R.P.; Marshall, A.G.; Qian, K.; Robbins, W.R. Identification of acidic NSO compounds in crude oils of different geochemical origins by negative ion electrospray Fourier transform ion cyclotron resonance mass spectrometry. *Org. Geochem.* **2002**, *33*, 743–759. [[CrossRef](#)]
41. Wu, Z.; Jernström, S.; Hughey, C.A.; Rodgers, R.P.; Marshall, A.G. Resolution of 10,000 compositionally distinct components in polar coal extracts by negative-ion electrospray ionisation Fourier transform ion cyclotron resonance mass spectrometry. *Energy Fuels* **2003**, *17*, 946–953. [[CrossRef](#)]
42. Finch, B.E.; Stefansson, E.S.; Langdon, C.J.; Pargee, S.M.; Blunt, S.M.; Gage, S.J.; Stubblefield, W.A. Photo-enhanced toxicity of two weathered Macondo crude oils to early life stages of the eastern oyster (*Crassostrea virginica*). *Mar. Pollut. Bull.* **2016**, *113*, 316–323. [[CrossRef](#)] [[PubMed](#)]
43. Cho, Y.; Ahmed, A.; Islam, A.; Kim, S. Developments in FT-ICR MS instrumentation, ionisation techniques, and data interpretation methods for petroleomics. *Mass Spectrom. Rev.* **2015**, *34*, 248–263. [[CrossRef](#)] [[PubMed](#)]
44. Pradyot, P. *A Comprehensive Guide to the Hazardous Properties of Chemical Substances*; Wiley & Sons: New York, NY, USA, 2007; pp. 161–568.
45. Khalaf, S.; Shoqeir, J.H.; Lelario, F.; Bufo, S.A.; Karaman, R.; Scrano, L. TiO_2 and Active Coated Glass Photodegradation of Ibuprofen. *Catalysts* **2020**, *10*, 560. [[CrossRef](#)]